AIAA JOURNAL
Vol. 33, No. 8, August 1995

Investigation of Flow at Leading and Trailing Edges of Pitching-Up Airfoil

C. Shih,* L. M. Lourenco,† and A. Krothapalli‡
Florida A&M University and Florida State University, Tallahassee, Florida 32316-2175

The dynamic stall process of an NACA 0012 airfoil undergoing a constant-rate pitching-up motion is studied experimentally in a water towing tank facility. This study focuses on the detailed measurement of the unsteady separated flow in the vicinity of the leading and trailing edges of the airfoil. The measurements are carried out using the particle image velocimetry technique. This technique provides the two-dimensional velocity and associated vorticity fields, at various instants in time, in the midspan of the airfoil. Near the leading edge, large vortical structures emerge as a consequence of van Dommelen and Shen type separation and a local vorticity accumulation. The interaction of these vortices with the reversing boundary-layer vorticity initiates a secondary flow separation and the formation of a secondary vortex. The mutual induction of this counter-rotating vortex pair eventually leads to the ejection process of the dynamic stall vortex from the leading-edge region. It is found that the trailing-edge flowfield only plays a secondary role on the dynamic stall process.

Introduction

WITH recent interest in the development of highly maneuverable aircraft, much emphasis has been placed on understanding of unsteady separated flows that occur over a wing pitching up rapidly from zero to high angle of attack. Such a rapid change in the angle of attack will result in an unsteady flowfield which is significantly different from that of a wing undergoing a quasi-steady-state motion. The difference is mainly due to the initiation of local unsteady boundary-layer separation and its subsequent interaction with the external flow. The strong inviscid/viscous interaction eventually leads to massive boundary-layer separation and formation of large-scale vortical structures, commonly referred to as dynamic stall vortices, which dominate the unsteady flow behavior over the wing. Since these vortices induce large suction forces on the upper surface of the wing, they are critical to its aerodynamic performance.[1,2] A careful management of these energetic structures can result in an effective control scheme to improve the flight envelope.[3] Many references that deal with the dynamic stall process can also be found in a recent review article by Doligalski et al.[4]

The dynamic stall process as described in Shih et al.[5] and more recently by Doligalski et al.[4] includes the following main features. The stall process is initiated by the unsteady boundary-layer separation near the airfoil's leading edge. During rapid pitching-up motion of the airfoil, vorticity production is greatly enhanced by the favorable pressure gradient at the leading edge. At the same time, vorticity accumulates locally due to the slowdown of downstream convection process caused by the presence of an adverse pressure gradient and local boundary-layer flow reversal. The accumulation process is eventually interrupted by a sudden emergence of unsteady flow separation, with the immediate release of the accumulated vorticity into the outer flow. The eruption of boundary-layer vorticity triggers a sequence of spontaneous events such as local viscous/inviscid boundary-layer interaction, formation and convection of large energetic vortices, and, finally, the "stall." Thus, in order to understand the dynamic stall process, a better physical understanding of the unsteady boundary-layer separation is necessary.

A significant advance in the understanding of the unsteady separation process was made by van Dommelen and Shen[6] (VDS), who used an innovative Lagrangian approach to study the boundary-layer separation over an impulsively started cylinder. They found no evidence of the emergence of singular behavior near the separation point as usually encountered by the traditional boundary-layer analysis. This allowed them to examine in detail the evolution of the unsteady separation structure. They concluded that the strong adverse pressure gradient is the initial trigger for the onset of flow reversal along the surface. However, as the fluid particles approach the separation point, the convective terms become dominant compared to the viscous and pressure gradient terms. As a result, along the zero vorticity line, Burger's equation dominates immediately before separation. Physically, the fastest reversing fluid particles quickly approach the slower moving particles and create a local particle collision. Because of the restraint of the solid surface, the particles will be propelled away from the wall as a consequence of the rapid compression along the wall and "separation" occurs. Under inviscid assumption, the particles conserve vorticity, and the movement of the particles away from the wall signifies the outward distortion of the zero vorticity line. As will be shown later in the results section, this distortion provides a deterministic perturbation to destabilize the local vorticity distribution which results in the formation of large vortical structure. The development of this vortex and its induced secondary separation leads to its ejection from the surface. The dynamic stall process is then initiated by the inviscid/viscous interaction between the vortex and the outer flow.

Like most boundary layer formulations, the VDS model implicitly assumes infinitely high Reynolds number. However, the present water towing tank experiments were performed at relatively low Reynolds numbers of 5,000 and 25,000. Therefore, it is necessary to consider the effect of Reynolds number on the evolution of unsteady separation. According to the VDS model, the unsteady separation is initiated by the local adverse pressure gradient and later governed by the inertial effect as modeled by Burger's equation. Thus, the onset of the unsteady separation structure is virtually inviscid and independent of the Reynolds number. As a matter of fact, it has been speculated that the generic characteristics of an unsteady separated flow are fairly universal and independent of the Reynolds number and external flow conditions. Therefore, the results from a low Reynolds number experiment can be applied to higher Reynolds number flow conditions with confidence. On the other hand, because of the Reynolds number effect, appreciable differences in time and length scales of the separation structure are expected. For example, the separation structure of a low Reynolds number flow evolves faster as compared to a high Reynolds number case.[7] Moreover, the stronger viscous diffusion of a low Reynolds number flow will thicken the boundary layer and thereby attenuate the explosive nature of the unsteady separation. None of these effects, however, are expected to alter the intrinsic behavior of the unsteady separation structure as described by van Dommelen and Shen.[6] It is, therefore, possible

Received May 26, 1994; revision received Jan. 4, 1995; accepted for publication Jan. 4, 1995.

*Associate Professor. Member AIAA.
†Professor. Member AIAA.
‡Don Fuqua Professor and Chair. Associate Fellow AIAA.

to extend the present results to flows at much higher Reynolds numbers.

The dynamic stall process just described is mostly based on theoretical/computational studies[8–10] and flow visualization and/or pressure measurements.[11–13] To date, except in a few instances,[5,14] most of the unsteady separated flowfield measurements have employed traditional techniques, such as hot-wire and laser Doppler anemometer. These single-point measurement techniques cannot capture the overall evolution of the spatial and temporal flowfields, which are essential in the understanding of the interaction between the large-scale vortices and the local boundary layer in a separated flow. To overcome these limitations, the present study employs the particle image velocimetry (PIV) method. This whole-field technique can provide the instantaneous two-dimensional velocity field and the associated vorticity field in a selected plane of the flowfield. This technique has been successfully used in describing global features of the dynamic stall process over a pitching-up airfoil both in high[15] and low[5] speeds. A detailed description of the PIV technique can be found in Lourenco et al.[16] and Adrian.[17]

With the use of the PIV technique, this paper provides detailed velocity and vorticity field measurements to describe the development of the unsteady flow over the leading edge of a pitching-up airfoil. The role of the trailing-edge flow on the dynamic stall process is also examined. Main parameters that govern this flowfield include the airfoil geometry, the freestream Reynolds number, and the nondimensional pitch rate. In the present work an NACA 0012 airfoil was used. Two different Reynolds numbers of 5,000 and 25,000, based on the chord of the airfoil C and the freestream velocity U_∞, were investigated. Experiments were conducted at a dimensionless pitch rate, $\alpha^+ (= \alpha C/U_\infty)$, of 0.131.

Experimental Facility and Instrumentation

Experiments were performed in a water towing tank facility with dimensions of 3.4 m in length and 0.6 × 0.5 m in cross section. A computer-interfaced Anorail linear motor system was used to drive the towing carriage. This system allows fine control of the towing velocity. In the present investigation, the velocity of the towing carriage was varied from 5 to 25 cm/s. The corresponding Reynolds number, based upon the airfoil's chord, was varied from 5,000 to 25,000. The airfoil's pitching motion was controlled by a programmable Klinger stepping motor control unit. Three moving platforms, one for model mounting, one for the rotating mirror system used to create the pulsed laser illumination, and one for image recording, were synchronized using a gear/belt system (Fig. 1). All motions were controlled by a desktop IBM PS/2 model 70 computer. The pulsed laser sheet was created by means of a 24-faceted rotating mirror system. This mirror swept a 5-W Argon laser beam into a laser sheet which was projected along the midspan of the airfoil, providing multiple particle image illumination required for the PIV image recording.

The PIV technique can be regarded as a quantitative flow-visualization method that is capable of providing accurate two-dimensional instantaneous velocity and vorticity fields (please see Lourenco et al.[16] for a detailed description). To resolve the directional ambiguity of the velocity vector, a velocity bias technique

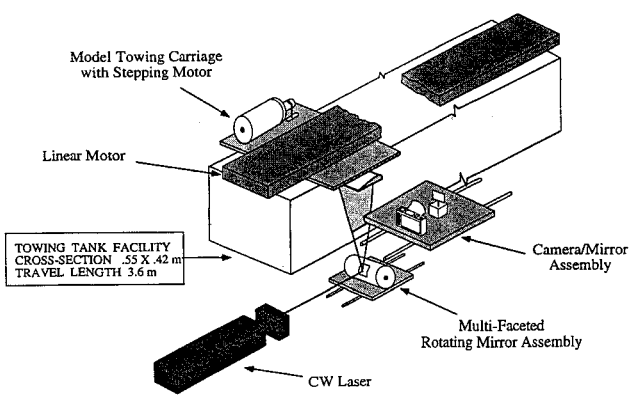

Fig. 1 Schematic sketch of the towing tank and the PIV facility.

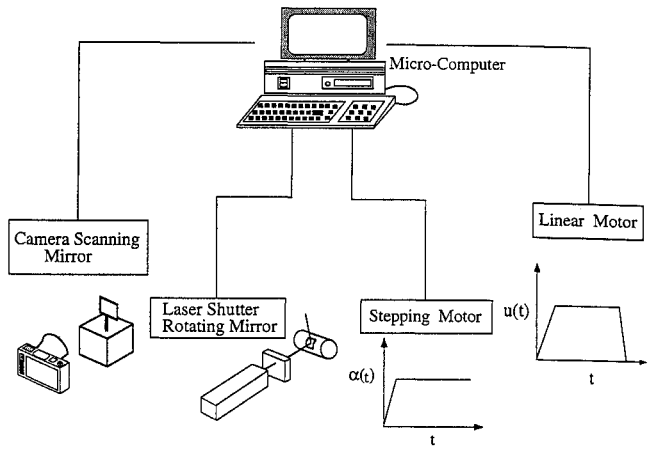

Fig. 2 Control system of the towing tank and PIV image acquisition.

was used. A uniform reference motion is added to the flow, thus superposing a velocity shift to the real flowfield. A properly chosen shift can insure that all image displacements occur in the same direction, thereby eliminating the ambiguity. The true flowfield can be recovered later by removing this artificial shift from the raw velocity data. In this work, a rotating mirror (General Scanner Model CX660) was used to produce the image shift. Optical and digital image-processing techniques were used to convert the acquired PIV photographic records into local velocity data. This process uses a focused laser beam to interrogate a small area of the multiple exposed photographic film. The interrogation beam diameter corresponds to an equivalent physical probe size of 0.625 mm. The diffraction pattern produced by the coherent illumination of the correlated multiple images on the film generates Young's fringes. These fringes have an orientation that is perpendicular to the direction of the local velocity vector and a spacing inversely proportional to the magnitude of the velocity. A fully automated PIV image processing bench, controlled by the Fluid Flow Diagnostics Mark II program was used to digitize and process the fringe images. The PIV measurements have been calibrated by examining the uniform velocity field created by towing the camera carriage at a known constant speed. The velocity is found to be accurate to within 1.5% of the reference velocity. The associated out-of-plane vorticity field is computed from the PIV velocity data by means of a central finite difference scheme and is normalized by the airfoil's chord and the freestream velocity. To accurately capture the fine structures near the surface of the airfoil, the PIV data were processed with a very small step size (the corresponding step size in the physical plane is 0.5 mm, or 0.5% chord length, in both directions). All data presented are instantaneous flowfields without the use of a phase-averaging technique. In general, the global events described in this paper are very repeatable between different experimental runs. However, because of the unstable nature of an unsteady separated flow, the timing of the occurrence of these events cannot be duplicated exactly. Please refer to Shih et al.[5] for a more detailed discussion concerning the repeatability of the experiment.

Metallic coated particles (TSI model 10087), with an average diameter of 11 μm and a specific gravity of 2.6, were used as flow tracers. A phase-triggered 35-mm single-lens reflex camera (Nikon F-3) was used to record the image at a controllable rate, ranging from 1 frame/s to a maximum rate of 6 frames/s. The magnification of the recording system (image to object ratio) was calibrated to be 0.5. Synchronization between components was accomplished by means of a Tektronix modular electronics system. This system also provided the phase reference between the motion of the airfoil and the PIV photographic timing sequence (Fig. 2).

Experimental Results and Discussion

The global flow development was described earlier by Shih et al.[5] using a sequence of PIV velocity and associated isovorticity fields under the same experimental conditions. A general description of the flowfield at the leading and trailing edges is given in this section. The solid isovorticity contours represent vorticity rotating in a clockwise sense; the dotted contours represent counterclockwise

vorticity. The focus of the following discussion is on the detailed mechanics of the flow at the leading and trailing edges.

Unsteady Separation and the Formation of the Leading-Edge Vortex

The emergence of unsteady separation up to the formation and ejection of the dynamic stall vortex, is shown in detail in Figs. 3a–3f, where $t^+ = tU_\infty/C$ is the nondimensionalized time. These pictures cover approximately the region from the leading edge to 60% chord downstream. The airfoil's quarter-chord position is identified on the plot for reference purposes.

As the airfoil pitches beyond its static stall angle, a strong leading-edge suction pressure peak is developed by the presence of a rapidly accelerating fluid stream flowing over the nose. Downstream of the nose region up until the airfoil's trailing edge, flow reversal develops near the surface where an increasingly adverse pressure gradient dominates. However, unlike the steady flow, the external flow stream continues to follow the airfoil's contour, and there is no apparent "breakaway" of the boundary-layer flow from its surface (Fig. 3a). It is necessary to point out that, although there is a reversing flow layer extending from the trailing edge over the entire airfoil, the flow reversal near the leading edge and the eventual initiation of unsteady separation are essentially local flow phenomena. In other words, all reversing fluid particles in the leading-edge separation region originate locally near the leading-edge region (note: leading-edge region is loosely defined as the region extending from the airfoil's nose to about 30% chord). This is in contradiction to the suggestion made in some earlier observations that the dynamic stall process is triggered by the arrival of a reversing flow which originates at the trailing edge. This contradiction can be resolved using a simple time/space development calculation as follows. First, assume the flow reversal starts at the instant when the airfoil approaches its static stall angle, $\alpha = 10$ deg, or at $t^+ = 1.33$ for this set of data. For a fluid particle that moves at an estimated averaged reversing speed of approximately 20% of the freestream velocity, it would have traveled for merely 27% of the chord until the time $t^+ = 2.69$ when the leading-edge separation process is already initiated (Fig. 3c). Therefore, there is simply not enough time for the trailing-edge flow to reach the nose region. Consequently, the trailing-edge flow does not have a direct impact on the separation process. This has an important implication because it suggests that the influence from the trailing edge is an indirect one and only through the increase of global circulation of the airfoil by shedding counter-rotating vorticity into the wake. Therefore, a local flow control such as blowing or suction in the leading-edge region will be sufficient to manipulate the behavior of the flow at this stage. Any modification near the trailing edge should have no significant influence on the early development of the leading-edge flow separation.

Because of the reversing flow, the upper part of the boundary layer near the trailing-edge area moves away from the surface, forming a local "free" shear layer. This shear layer is subjected to inflectional point instabilities and immediately rolls up into several large-scale vortices; one such vortical structure can be seen near the midchord region in Fig. 3b. This structure quickly convects downstream and detaches itself from the midchord region (Fig. 3c). The consequence of this departure is that it forces the leading-edge shear layer to reattach and, at the same time, slows down the downstream vorticity convection from the leading edge (Figs. 3b and 3c). Basically, the leading-edge region has been temporarily isolated from the direct influence of the rest of the flowfield, and the subsequent evolution is predominantly controlled by the emergence of local boundary-layer separation and the resulting vorticity dynamics.

The leading-edge boundary layer is propelled away from the airfoil's surface by the reversing fluid layer near the surface which is driven by the adverse pressure gradient. Unlike the steady separation, the outer flow remains unaffected by the flow reversal and continues to follow the airfoil's contour. Consequently, a local free shear layer emerges between the displaced leading-edge boundary layer and the reversing fluid layer. This shear layer can then be subjected to inflectional instability and leads to the generation and growth of individualized vortical structures (Figs. 3a–3f). Before the onset of unsteady separation, these structures are small with a scale comparable to the local shear layer thickness. However, under the influence of the increasing adverse pressure gradient, the local reversing flow begins to accelerate rapidly inside the leading-edge region. This leads to the emergence of a VDS interaction such that the fastest reversing particles quickly approach and, eventually, collide with the slower moving particles ahead of them. This collision takes place along the zero vorticity line as indicated by the interface between solid (clockwise) and dotted (counterclockwise) isovorticity lines, and results in a local movement of the particles away from the wall. Consequently, the local zero vorticity interface is displaced away from the wall. This vorticity line distortion initiates the separation process (Figs. 3b–3d), and appears to agree with the overall concept of the van Dommelen and Shen model.

Unlike the traditional shear layer instability mechanism which selectively amplifies random perturbations in the initial region to develop into organized vortical structures, the deformation triggered by the VDS interaction provides a deterministic perturbation to the local vorticity distribution (see Fig. 4 for a conceptual description of this process). The upward displacement of counterclockwise vorticity into the outer shear layer, where clockwise vorticity dominates, makes the local vorticity arrangement highly unstable. Under their mutual induction, the interface between regions of concentrated vorticity of opposite sign quickly undergo further self-induced deformation. The downstream interface stretches into a peak whereas the upstream interface develops into a valley as shown in Fig. 4. Eventually, this spontaneous deformation evolves into a spike-like eruption which propels more counter-rotating vorticity into the external flow stream. The narrow-band eruption is consistent with the terminal boundary-layer structure as predicted by the VDS interaction.[18] It is noted that, although the onset of VDS interaction is fairly deterministic, a simple definition for its timing, location, and physical scale is not possible. Timing, location, and physical scales are usually determined by many parameters, such as the Reynolds number, dimensionless pitch rate, airfoil's nose shape, Mach number, etc. However, for a given set of flow conditions, this distortion is well defined and predictable. For a detailed discussion of the unsteady separation process please refer to van Dommelen.[18] Since the emergence of this perturbation is deterministic, it is, therefore, possible to control the separation process by proper management of this local interaction.

Immediately after the distortion of the zero vorticity line, discrete vortical structures evolve very quickly. During the short period of time spanning from the appearance of the first individualized vortical structure in the shear layer (Fig. 3a) to the emergence of the dynamic stall vortex (Fig. 3h), the size of the shear layer vortex increases dramatically. For example, as shown in Fig. 3b, four of the leading-edge shear layer vortices appear to undergo a collective merging process and coalesce into a much large structure as shown in Fig. 3c. This extraordinarily rapid growth cannot be explained by the typical Kelvin–Helmoholtz instability mechanism. Two possible models are suggested: 1) The zero vorticity line distortion triggered by the VDS interaction provides a strong perturbation with a wavelength much longer than the local shear layer thickness. This distortion displaces the shear layer into an unstable arrangement so that many shear layer vortices can undergo merging through mutual induction and eventually form a large vortical structure. A similar nonlinear instability mechanism has been referred to as collective interaction by Ho and Nosseir[19] in their study of an impinging jet in self-sustained oscillation. They found that the collective interaction always leads to a higher spreading rate of the shear layer and the formation of a large coherent structure. 2) During separation, the instantaneous reversing boundary-layer flow (U_r) can be of the same order of magnitude as the outer shear layer velocity (U_s). The local shear layer velocity ratio, defined as $(U_s - U_r)/(U_s + U_r)$, can well exceed the critical ratio of 1.315 for the theoretical transition of shear layer instability from convective to absolute mode.[20] Therefore, the local shear layer can become self-excited at a discrete frequency with higher amplification. In the present case, the VDS interaction provides the initial perturbation, and the shear layer undergoes self-excited oscillations. Consequently, the shear layer vorticity quickly coalesces into a large structure, and leads to the formation of the dynamic stall vortex. Both models appear to be able to explain the relatively high growth rate of the separated leading-edge shear

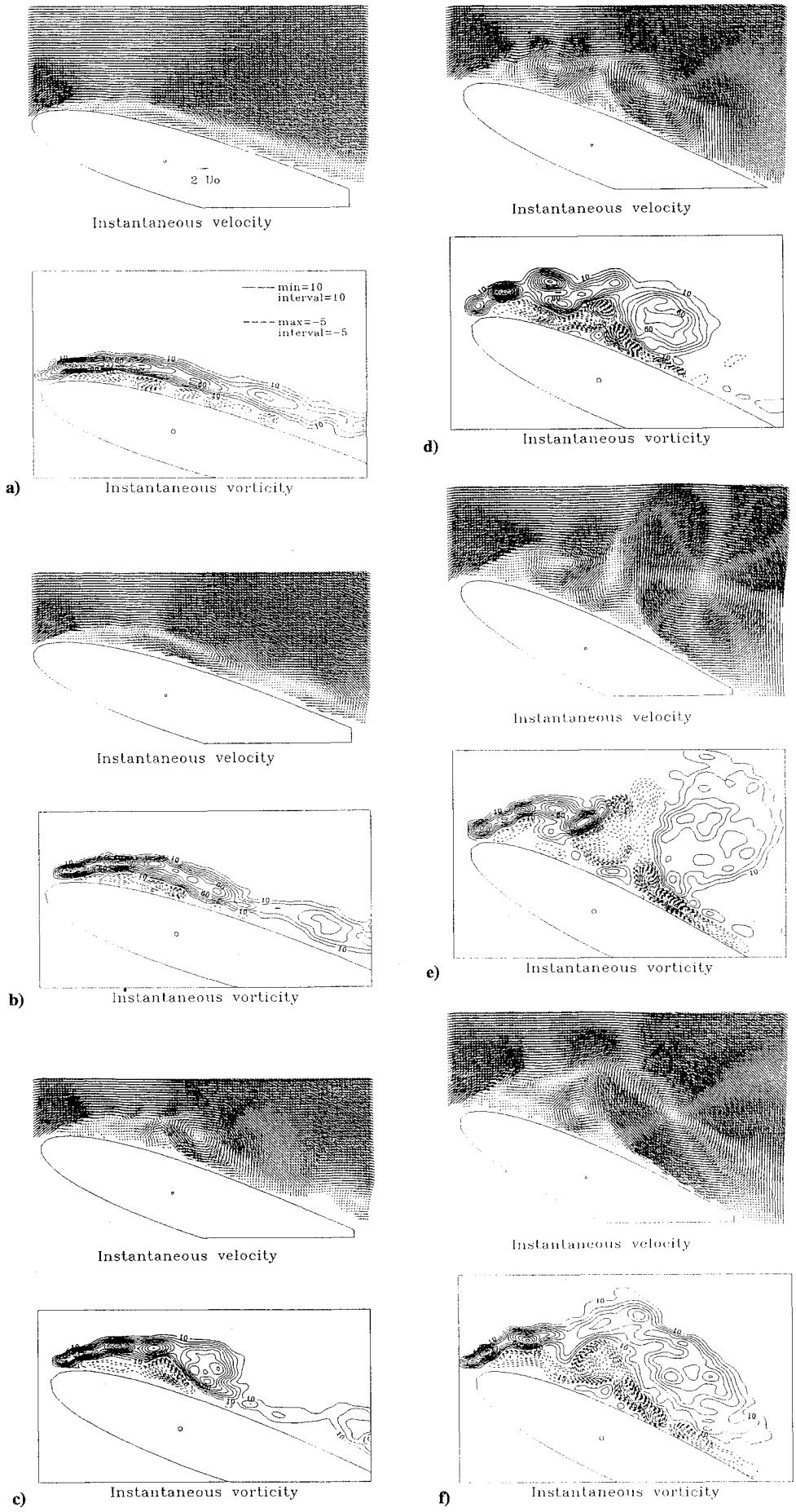

Fig. 3 Time sequence of the instantaneous velocity and vorticity fields, leading-edge region: a) $t^+ = 2.35$, $\alpha = 17.6$ deg, b) $t^+ = 2.52$, $\alpha = 18.9$ deg, c) $t^+ = 2.69$, $\alpha = 20.2$ deg, d) $t^+ = 3.03$, $\alpha = 22.7$ deg, e) $t^+ = 3.37$, $\alpha = 25.3$ deg, and f) $t^+ = 3.54$, $\alpha = 26.6$ deg.

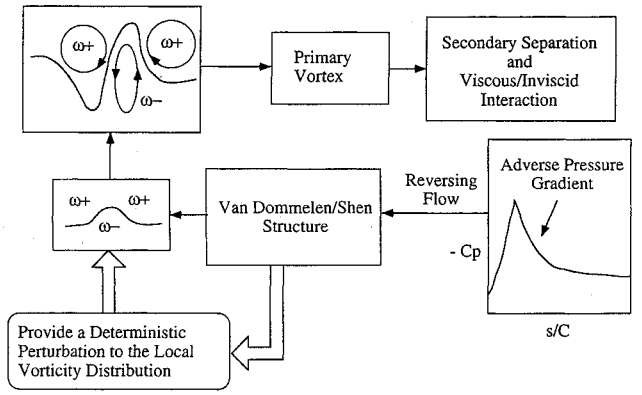

Fig. 4 Proposed time development of the unsteady separation process and the formation of the dynamic stall vortex.

layer and the formation of the dynamic stall vortex. It is also possible that these two mechanisms are complementary to each other. More systematic study is necessary to confirm the validity of these suggestions. A more detailed description of the role of absolute and global instabilities on the dynamic stall process is described by Shih et al.[21]

Secondary Separation and Vortex Interaction

During the separation process, clockwise vorticity is continuously being generated at the airfoil's nose and is being fed into the separating shear layer, resulting in further accumulation of vorticity and the strengthening of the primary vortex. This agglomeration process slows down the vorticity convection and induces flow attachment downstream of the leading-edge region (Figs. 3b and 3c). Near the airfoil's midchord, a vortex convects toward the trailing-edge region which will eventually couple with a trailing-edge vortex shed from the lower surface to form the trailing-edge vortex pair. This interaction will be described in a later section.

At the next instant, Fig. 3d, under the influence of the primary vortex, the reversing flow also separates from the surface and develops into another local free shear layer, carrying vorticity of counterclockwise sense. This shear layer quickly rolls into a secondary vortical structure, (Figs. 3d and 3e). In the meantime, the primary vortex continues to grow in size and strength, and a counter-rotating vortex pair is formed (Fig. 3f). The secondary vortex is smaller with a circulation that is 35% of the primary vortex at this instant. However, the secondary vortex is much more compact in size and, actually, has a relatively higher vorticity concentration. Therefore, the secondary vortex is able to move the primary vortex upward away from the surface where it encounters a faster convection velocity and moves rapidly downstream, initiating the dynamic stall process. On the other hand, the primary vortex also imposes strong interaction on the secondary structure which eventually leads to the eruption of the reversed boundary-layer flow into a spike-like structure. This eruption of counterclockwise vorticity cuts off the supply of vorticity from the leading-edge shear layer into the primary vortex (Fig. 3f). Consequently, the dynamic stall vortex is formed and begins to move away from the leading-edge area. This type of strong inviscid/viscous interaction is a generic characteristic of an unsteady separated flow as suggested by Shih et al.[5] and Ho and Didden.[22] A recent review by Doligalski et al.[4] describes admirably the presence of such an unsteady separated flow structure in flows involving vortex interactions with walls.

To examine the dynamics of the leading-edge separated vortex, the identity of each individual vortical structure has to be clearly defined. This is not easy since the vortical structure is not completely separated from the leading-edge shear layer until very late during the vortex formation stage (Fig. 3). Therefore, a subjective identification is inevitable. From the vorticity contour plots, it is always possible to visually identify a vortex as the region where highly concentrated vorticity is enclosed by closed isovorticity contour lines. If one accepts the concentrated vorticity region as a vortex, then the strength of this vortex is determined by its circulation, $\Gamma = \int \omega \, dA$, where the integration is taken inside the enclosed area, and ω is the vorticity. This is a measure of the instantaneous strength of the vortex. A low-threshold vorticity integration limit of 5% of the local maximum vorticity level is chosen to eliminate the influence from the background and the reversed vorticity region. The convecting motion of the vortex can be characterized by examining its velocity of convection. The convection velocity of the vortex is defined as the averaged velocity of the integrated vorticity carried by the vortex, that is,

$$u_c = \frac{1}{\Gamma}\int u\omega \, dA \qquad \text{and} \qquad v_c = \frac{1}{\Gamma}\int v\omega \, dA$$

where u_c and v_c are calculated in a reference frame moving with the airfoil; u_c measures the downstream convection velocity and v_c measures the normal velocity of the vortex relative to the airfoil's surface, respectively. The evolution and interaction of the leading-edge vortex system can be studied by following the development of the strength and convection speed of the primary vortical structure by integrating the vorticity data from Figs. 3b–3f.

Figure 5a shows the variation of the circulation of the leading-edge vortex. Although there is no distinguishable primary vortical structure in Fig. 3b when $t^+ = 2.52$, the integration of the circulation of the four small structures inside the shear layer is included for comparison. The collective circulation of these four vortices is calculated to be approximately equal to the circulation of the primary vortex at the next instant, $t^+ = 2.69$, when it first emerges. This confirms our previous observation that the formation of the vortex results from the collective merging of the vortices inside the shear

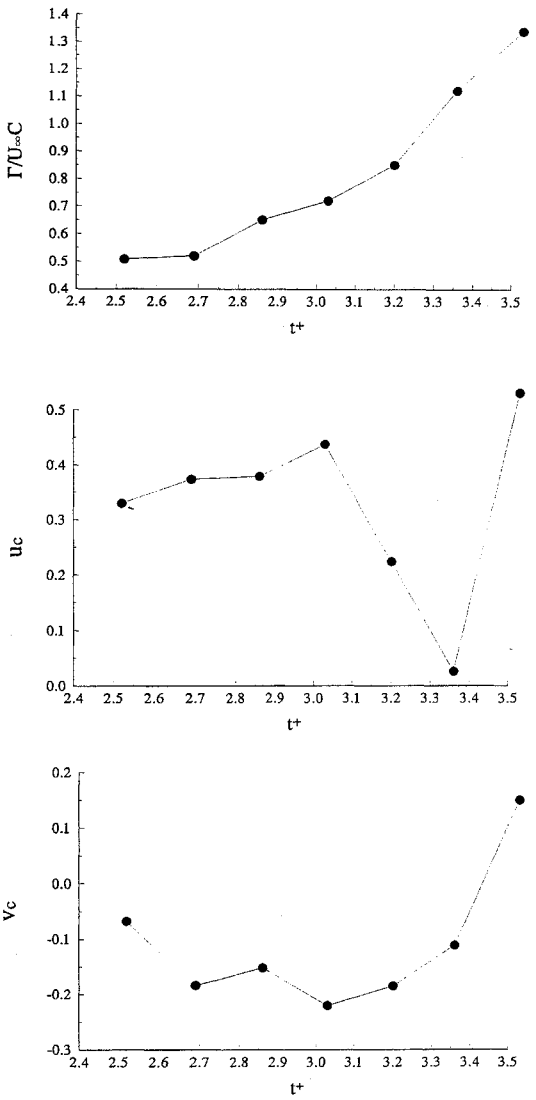

Fig. 5 Time evolution of the circulation and the convection velocity of the dynamic stall vortex.

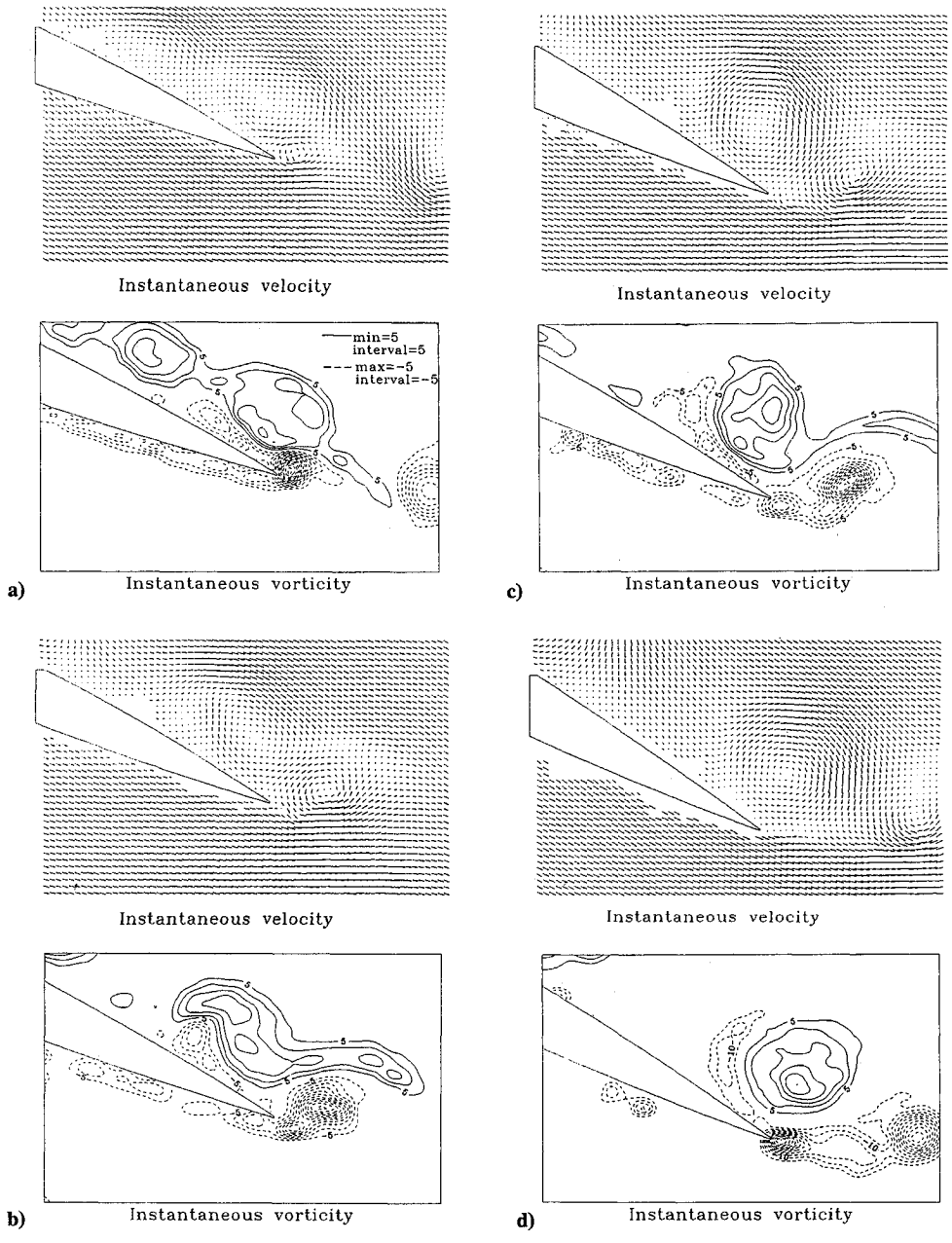

Fig. 6 Time sequence of the instantaneous velocity and vorticity fields, trailing-edge region, early stage development: a) $t^+ = 2.87$, $\alpha = 21.7$ deg, b) $t^+ = 3.21$, $\alpha = 24.3$ deg, c) $t^+ = 3.38$, $\alpha = 25.6$ deg, and d) $t^+ = 3.55$, $\alpha = 26.9$ deg.

layer. From the development of the circulation data, the growth of the primary vortex can be separated into two stages. During the first stage, the strength of the primary vortex increases immediately after the initiation of the unsteady separation structure (Figs. 3b–3d, $t^+ =$ 2.52–3.03). It is believed that the strong nonlinear instability development of the separated shear layer is responsible for the growth of the primary vortex during this stage. As a consequence of the intrusion of the reversed boundary-layer vorticity into the outer shear layer, another large-scale vortex develops upstream of the separation structure (Fig. 3d). During this period, the separated shear layer continues to feed vorticity into these two structures. However, there is no significant interaction between these vortices during this stage. The second stage starts when these two structures begin to interact. Under their mutual induction, these two vortices roll around each other and eventual merge into one single vortex (Figs. 3e and 3f, $t^+ = 3.03$–3.54). It can be seen, at the same time, that this strong interaction forces the eruption of the reversed boundary layer into a strong counter-rotating secondary structure (Fig. 3f). This secondary structure has a circulation that is 35% of the primary vortex at this time. However, due to its compactness, the local vorticity concentration is actually higher than that of the primary vortex. Consequently, under its induction, the primary vortex is displaced away from the surface and starts to convect downstream. During the second stage, the circulation of the primary vortex increases with a high rate as a result of this large-scale merging process.

This two-stage evolution can be more easily identified from the measurement of the vortex convection velocity as presented in Figs. 5b and 5c. During the first stage, the primary vortex convects downstream at an almost constant velocity u_c of 36% of the freestream velocity. During the same period, the vortex seems to move gradually toward the surface as indicated by the negative value of the normal convection velocity v_c. The second stage starts with a sudden decrease of the downstream convection velocity. As discussed previously, two large-scale vortices are undergoing a merging process. As they roll around with respect to each other, their collective convection velocity decreases significantly. As a matter of fact, the merging vortex system becomes virtually standing still at one instant, $t^+ = 3.36$. The merging of these two structures increases considerably the strength of the primary vortex and, correspondingly, prompts the accumulation of the secondary vortex. Moments

later, $t^+ = 3.53$, the newly formed vortex is ejected away from the airfoil surface because of the induction from the secondary vortex. This upward movement can be characterized by the sudden increase of the normal convection velocity of the primary vortex (Fig. 5c). To estimate quantitatively the upward velocity of the primary vortex as it is induced by the emergence of the secondary vortex, the Biot–Savat law of vortex induction is used. The induction velocity can be computed as $u_I = \Gamma_s/(2\pi r)$, where Γ_s is the total circulation of the secondary vortex and r is the distance between the secondary vortex and the primary vortex. The circulation of the secondary vortex is estimated to be 0.38 $U_\infty C$ as calculated using 35% of the strength of the primary vortex at this instant (Fig. 5a). The distance between these two structures is approximately 17% of the chord. Hence, the induction velocity is found to be in the order of 35% of the freestream velocity. This induced value is comparable to the total increase of v_c during a period from $t^+ = 3.2$–3.54 when the secondary vortex is collecting its strength (Figs. 3d and 3e). Therefore, it is concluded that the primary vortex is ejected out of the surface as a result of the upward induction by the secondary structure. As a result of this outward motion, the vortex is moved farther into the freestream where it experiences the faster downstream convection. The instantaneous convection velocity of the vortex is suddenly increased to as high as 50% of the freestream velocity (Fig. 5b). At the same time, the ejection of the secondary vortex into a spike-like structure cuts off the primary vortex from the leading-edge shear layer and completes the formation of the dynamic stall vortex (Fig. 3f).

Implication for Flow Control

It is certainly more difficult to devise an effective scheme to manipulate this energetic structure after it moves away from the leading edge than at its early stage of development. Therefore, it is reasonable to assume that the stage most accessible to manipulation would be the vortex formation process as described in the preceding section. The existence of a deterministic VDS interaction suggests the possibility of controlling the separation process in a well-defined fashion. If one can delay or remove the particle collision process at the onset of the separation, then the formation of the large-scale separated structures and their subsequent evolution can be delayed or eliminated. On the other hand, the strong interaction between the primary vortex and the secondary separated vortex seems to be another promising candidate from the viewpoint of effective flow control. Several numerical simulation studies have been developed to examine the possibility of controlling the leading-edge separated flow.[23,24] Their results show that the ejection of the leading-edge vortex can be delayed significantly by applying flow suction at the leading-edge region. It is believed that, through suction, the reversing flow under the vortex is kept close to the surface, which either delays or eliminates the eruption of the VDS-type of separation. Without this perturbation, the nonlinear instability mechanism that leads to the formation of the primary vortex cannot be initiated. At the same time, this modification also prevents the emergence of the secondary separation and the highly unstable counter-rotating vortex pair arrangement. Consequently, the stall process can be delayed.

Trailing-Edge Flow

The role of the trailing edge in the initial vortex formation has been shown in the preceding section to be unimportant, especially for cases corresponding to high pitch rates. However, as a consequence of continuous shedding of counter-rotating vorticity into the wake, the trailing edge has an indirect but considerable influence on the global flow dynamics, that is, it can increase the overall circulation around the airfoil. This circulation increase results in more vorticity accumulation near the leading edge which eventually leads to the formation of stronger vortices. On the other hand, at later stages of the dynamic stall, the influence of the trailing-edge flow may increase significantly when the primary vortex approaches the trailing edge.

The onset of the trailing-edge separation can be seen as the upper boundary-layer flow separates and accumulates into discrete vortices (Fig. 6a). Two of these structures can be observed to undergo a merging process into one single vortex (Figs. 6b and 6c). This local accumulation increases the shedding of counterclockwise trailing-edge vorticity from the lower surface, which gradually

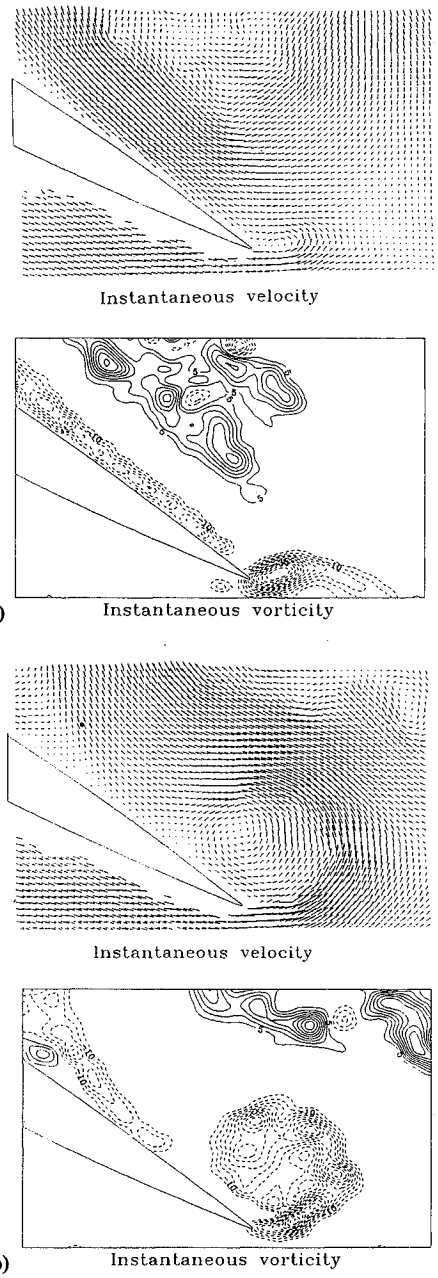

Fig. 7 Time sequence of the instantaneous velocity and vorticity fields, trailing-edge region, later stage development: a) $t^+ = 4.91$, $\alpha = 30.0$ deg and b) $t^+ = 5.59$, $\alpha = 30.0$ deg.

coalesces into a vortex rotating in the opposite sense. The upper surface shear layer vortex interacts with the reversed trailing-edge vortex to form a counter-rotating vortex pair as shown in Fig. 6c. These two counter-rotating vortices have comparable strength (their difference is less than 10%). Consequently, the mutual downward induction from these two vortices can stabilize the vortex pair and slow down its breakaway from the trailing edge (Figs. 6b–6d).

At a later stage during the stall process, as the primary vortex is approaching the trailing edge of the airfoil, strong flow reversal prevails along the upper surface (Fig. 7a). When the dynamic stall vortex reaches the trailing edge, it induces a local suction pressure which drives the lower surface separating layer across the wake into the upper surface. This lower surface shear layer vorticity quickly rolls into an intense counterclockwise vortex (Fig. 7b). The emergence of this vortex signifies the completion of the dynamic stall process and the subsequent sudden loss of vortex lift as the dynamic stall vortex departs from the trailing edge. From the integrated flow control point of view, the shedding of a strong vortex can be detected through surface probes at the trailing edge and can be utilized as a warning signature for the flow management system.

Summary

The flow past an airfoil pitching at a constant rate is studied in a water towing tank facility. Instantaneous velocity and associated out-of-plane vorticity fields were measured using the whole-field PIV technique. Special emphasis has been placed on the study of flow structure near the airfoil's leading- and trailing-edge regions. As the airfoil pitches well beyond the static stall angle, detailed analysis of the flow indicates that the unsteady separation process as described by van Dommelen and Shen leads to vortex formation at the leading edge. Strong inviscid/viscous interaction between the primary vortex and the reversed boundary-layer leads to a secondary separation and the formation of a secondary vortex of opposite sign. The mutual induction of the counter-rotating vortex pair triggers the breakaway of the vortex from the leading edge, at the same time, initiating the dynamic stall process. The evolution of the vortex dominates the later flow behavior.

The trailing-edge flow plays only an indirect role on the dynamic stall process. In the early stages of the process a counter-rotating vortex pair has been observed at the trailing edge. Their influence is mostly confined to the alteration of the global circulation around the airfoil. During the later stages of the process, as the primary vortex approach the trailing edge, a counter-rotating vortex is shed from the trailing edge indicating the completion of the dynamic stall.

Although not reported here, the data from a high Reynolds number (25,000) experiment show the same flow behavior as was described here.

Acknowledgments

This work is supported by the Air Force Office of Scientific Research under Contract AFOSR F49620-89-C0014. The authors wish to thank S. Shankar and Z. Ding for their contribution to the PIV data collection and analysis. We also would like to thank George Buzyna for his helpful suggestions during the preparation of the manuscript.

References

[1]McCroskey, W. J., "Unsteady Airfoils," *Annual Review of Fluid Mechanics*, Vol. 14, 1982, pp. 285–311.

[2]Carr, L. W., "Progress in Analysis and Prediction of Dynamic Stall," *Journal of Aircraft*, Vol. 25, No. 1, 1988, pp. 6–17.

[3]Herbst, W. B., "Supermaneuverability," *Proceedings of Workshop on Unsteady Separated Flow*, edited by Francis and Luttges, U.S. Air Force Academy, Colorado Springs, CO, 1984, pp. 1–9.

[4]Doligalski, T. L., Smith, C. R., and Walker J. D. A., "Vortex Interactions with Walls," *Annual Review of Fluid Mechanics*, Vol. 26, 1994, pp. 573–616.

[5]Shih, C., Lourenco, L., van Dommelen, L., and Krothapalli, A., "Unsteady Flow Past an Airfoil Pitching at a Constant Rate," *AIAA Journal*, Vol. 20, No. 5, 1992, pp. 1153–1161.

[6]Van Dommelen, L., and Shen, "The Spontaneous Generation of the Singularity in a Separating Laminar Boundary Layer," *Journal of Computational Physics*, Vol. 38, Nov.–Dec. 1980, pp. 125–140.

[7]Peridier, V. J., Smith, F. T., and Walker, J. D. A., "Vortex-Induced Boundary-Layer Separation. Part 2. Unsteady Interacting Boundary-Layer Theory," *Journal of Fluid Mechanics*, Vol. 232, Nov. 1991, pp. 133–165.

[8]Visible, M., "Dynamic Stall of a Constant-Rate Pitching Airfoil," *Journal of Aircraft*, Vol. 27, No. 5, 1990, pp. 400–407.

[9]Ghia, K. N., Yang, J., Osswald, G. A., and Ghia, U., "Study of the Role of Unsteady Separation in the Formation of Dynamic Stall Vortex," AIAA Paper 92-0196, Jan. 1992.

[10]Choudhuri, P. G., Knight, D. D., and Visbal, M. R., "Two-Dimensional Unsteady Leading-Edge Separation on a Pitching Airfoil," *AIAA Journal*, Vol. 32, No. 4, 1994, pp. 673–681.

[11]Acharya, M., and Metwally, M. H., "Unsteady Pressure Field and Velocity Production over a Pitching Airfoil," *AIAA Journal*, Vol. 30, No. 2, 1992, pp. 403–411.

[12]Jumper, E. J., Schreck, S. J., and Dimmick, R. L., "Lift-Curve Characteristics for an Airfoil Pitching at Constant Rate," *Journal of Aircraft*, Vol. 24, No. 10, 1987, pp. 680–687.

[13]Koochesfahani, M. M., and Smiljanovski, V., "Initial Acceleration Effect on Flow Evolution Around Airfoils Pitching to High Angles of Attack," *AIAA Journal*, Vol. 31, No. 8, 1993, pp. 1529–1531.

[14]Lee, G., Buell, D. A., Licurisi, J. P., and Craig, J. E., "Laser Holographic Interferometry for an Unsteady Airfoil Undergoing Dynamic Stall," *AIAA Journal*, Vol. 22, No. 4, 1984, pp. 504–511.

[15]Crisler, W., Krothapalli, A., and Lourenco, L. M., "PIV Investigation of High Speed Flow Over a Pitching Airfoil," AIAA Paper 94-0533, Jan. 1994.

[16]Lourenco, L., Krothapalli, A., and Smith, C. A., "Particle Image Velocimetry, *Lecture Notes in Engineering: Advances in Fluid Mechanics Measurements*, edited by M. Gad-el-Hak, Springer–Verlag, New York, 1989, pp. 128–199.

[17]Adrian, R. J., "Particle-Imaging Techniques for Experimental Fluid Mechanics," *Annual Review of Fluid Mechanics*, Vol. 23, 1991, pp. 261–304.

[18]Van Dommelen, L. L., "Lagrangian Description of Unsteady Separation," *Lectures in Applied Mathematics*, Vol. 28, American Mathematical Society, 1991, pp. 701–718.

[19]Ho, C.-M., and Nosseir, N. S., "Dynamics of an Impinging Jet. Part 1. The Feedback Phenomenon," *Journal of Fluid Mechanics*, Vol. 105, April 1981, pp. 119–142.

[20]Huerre, P., and Monkewitz, P. A., "Local and Global Instabilities in Spatially Developing Flows," *Annual Review of Fluid Mechanics*, Vol. 22, 1990, pp. 473–537.

[21]Shih, C., Krothapalli, A., and Lourenco, L., "The Role of Absolute Instability on Formation of Dynamic Stall Vortex," *Advances in Computational Methods in Fluid Dynamics*, FED-Vol. 196, edited by K. N. Ghia, U. Ghia, and D. Goldstein, American Society of Mechanical Engineers, 1994.

[22]Didden, N., and Ho, C. M., "Unsteady Separation in a Boundary Layer Produced by an Impinging Jet," *Journal of Fluid Mechanics*, Vol. 160, Nov. 1985, pp. 235–256.

[23]Yang, J., Ghia, K. N., Ghia, U., and Osswald, G. A., "Management of Dynamic Stall Phenomenon Through Active Control of Unsteady Separation," AIAA Paper 93-3284, July 1993.

[24]Van Dommelen, L., Tech. Rept., Dept. of Mechanical Engineering, FAMU/FSU College of Engineering, Florida A&M Univ. and Florida State Univ., FMRL TR-8, Tallahassee, FL, April 1993.